J Appl Electrochem (2008) 38:785–791
DOI 10.1007/s10800-008-9513-7

ORIGINAL PAPER

A potential method for electrochemical micromachining of titanium alloy Ti6Al4V

L. M. Jiang · W. Li · A. Attia · Z. Y. Cheng · J. Tang · Z. Q. Tian · Z. W. Tian

Received: 29 August 2007 / Revised: 31 January 2008 / Accepted: 31 January 2008 / Published online: 21 February 2008

Abstract The micromachining of complex three-dimensional microstructures (bulk micromachining) on metals can be applied to fabricate many novel devices for micro electromechanical system (MEMS), which will greatly benefit the development of MEMS. In this paper, a new electrochemical micromachining method named the confined etchant layer technique (CELT) was explored on the micromachining of the titanium alloy. Micro-scale trapezoidal slots were replicated on titanium alloy by using a mold with the corresponding negative microstructures (trapezoidal teeth). The machining resolution reached 0.503 μm. The electrochemical mechanisms involved in the process are analyzed and the parameters that influenced the machining resolution are discussed.

Keywords Bulk micromachining · Confined etchant layer technique · Etching · Titanium

A. Attia is on leave from Physical Chemistry Department, National Research Centre, El-Tahrir St., Dokki, Cairo, Egypt.

L. M. Jiang (✉) · A. Attia · J. Tang · Z. Q. Tian · Z. W. Tian
State Key Laboratory for Physical Chemistry of Solid Surfaces, Department of Chemistry, Xiamen University, Xiamen 361005, China
e-mail: lm-jiang@vip.sina.com

L. M. Jiang · W. Li · Z. Y. Cheng
School of Material Science and Engineering, Nanchang Hangkong University, Nanchang 330063, China

A. Attia
Physical Chemistry Department, National Research Centre, El-Tahrir St., Dokki, Cairo, Egypt

1 Introduction

So far silicon is still predominant among the materials used for micro electromechanical systems (MEMS). In recent years, more metals have been investigated for MEMS due to their excellent electrical and thermal conductivity and mechanical and magnetic properties [1–6]. However, up to now metallic MEMS components that have been fabricated are mainly nickel and copper with simple structures since the main micromachining technology is based on LIGA (an acronym from German words for lithography, electroforming, and molding) [7, 8] that can be applied to fabricate high-aspect-ratio bulk microstructure for Ni and Cu [9, 10]. Titanium is an important metal, but it is difficult to micromachine by LIGA due to the difficulty in electro- or electroless-deposition of titanium in the microstructured photoresist formed by X-ray photolithography, which is one of the key steps of the LIGA process. Furthermore, the complex three-dimensional (3D) microstructures without straight sidewalls are very difficult to machine by LIGA.

Ti and its alloys possess the best strength-to-weight ratio and corrosion resistance among metals. In contrast with Si, Ti and its alloys have much higher fracture toughness, better electrical conductivity and greater biocompatibility. Therefore, they are very attractive for MEMS uses. Although as a functional thin film material, Ti has long been used in the microelectronics industry where only patterning titanium thin film (known as surface micromachining) is needed [11, 12], it is rarely used in MEMS due to the difficulty of micromachining complex 3D microstructure with a high-aspect-ratio. Surface micromachining on Ti is easy to carry out by photolithography, electronic beam, ionic beam or reactive ion etching and so on; however, these techniques are difficult

to apply in micromachining complex 3D microstructure for Ti. As well as the techniques mentioned above for metal micromachining, other methods of interest such as through-mask electrochemical micromachining (EMM) [13–15] have been investigated and some useful microstructures have been obtained [16–18]. However, due to the isotropy of electrochemical dissolution of metals, undercutting inevitably takes place. Therefore, it is difficult to get high-aspect-ratio microstructures, especially for complex three-dimensional microstructures. In the 1980s, Bard's group invented scanning electrochemical microscopy (SECM) [19] and used it in micromachining of metals [20–22]. It generated etchant electrochemically on a microelectrode to etch the samples and was effective for etching of copper. Nevertheless, owing to the free diffusion of the etchant, its spatial resolution was limited. Recently, two new approaches for bulk micromachining of metals were proposed. One was ultrashort voltage pulses electrochemical machining reported by Schuster et al [23–26]. The other was anisotropic reactive ion etching with oxidation (ARIO) reported by Aimi et al. [27]. However, complex 3D microstructures are still difficult to micromachine by these methods.

In this paper we present an electrochemical bulk micromachining method named the confined etchant layer technique (CELT) [28–32] for micromachining titanium and its alloys. The fundamentals of CELT can be described as follows: The etchant is generated electrochemically on the surface of a machining tool or a mold with desired 3D microstructures. A specific scavenger is added to the electrolyte that captures the etchant within a very short duration so as to prevent the etchant from diffusing away from the mold surface. Thus, the etchant layer around the mold is kept so thin that its profile takes approximately the contour of the microstructures of the mold. When moving the mold until the etchant layer contacting the workpiece, the workpiece will be etched. By continuously approaching the mold to the workpiece with etching proceeding, an approximate mirror-image replica of the microstructures of the mold is obtained.

Theoretically, if the concentration of the scavenger is much greater than that of the etchant generated on the mold, it can be assumed that the scavenger concentration remains constant during the whole process and the scavenging reaction is of pseudo-first-order with rate constant ks. The thickness of the confined etchant layer (μ) can be estimated as: $\mu = (D/ks)^{1/2}$ [32], where D is the diffusion coefficient of the etchant in the solution.

The major advantages of CELT can be summarized as follows: it can be used to fabricate complex 3-dimensional micro- (or nano-) structures; it can control precisely the machining depth by controlling the moving distance of mold (through high precision PZT), rather than by approximately controlling the machining time as in photolithography; it can be used in a batch process with fewer steps than in photolithography. The possible destruction and denaturalization of the intrinsic structure beneath the machining surface usually caused by high-energy beam machining can be avoided. In our laboratory the replication of complex 3D microstructures has been achieved on the surface of GaAs, Si, copper and nickel with a nano or sub-micro resolution [28–31].

Here, micromachining on titanium related alloys is reported. Microstructures like trapezoidal slots are replicated on titanium alloy (Ti6Al4V) by using a mold with trapezoidal teeth. The electrochemical mechanisms involved in the process are analyzed in detail and the parameters influencing machining resolution are discussed.

2 Experiment

The titanium alloy to be etched was Ti6Al4V with 1 mm thickness. It was polished with alumina powder of 2 μm, 0.5 μm and 0.05 μm diameter successively, then rinsed with water and acetone in an ultrasonic bath, and finally washed with ultra pure water prior to use. The 3D mold on which the etchant is generated electrochemically was set as the working electrode in a three-electrode system. The counter electrode was a Fe wire ring surrounding the working electrode, and a saturated calomel electrode (SCE) was used as reference electrode. The workpiece (Ti6Al4V) was set at open-circuit in the solution. As the contact between the mold and workpiece would lead to anodic dissolution of the workpiece, a potentiometer was connected between them to detect the voltage change so as to judge whether they were contact or not. Great care should be taken to avoid contact between them as the mold approaches the workpiece surface. During the etching process, the mold was raised some distance and then lowered periodically to allow the solution between mold and workpiece to be refreshed. The mold used in this work was a silicon wafer containing some regular trapezoidal gear-like microstructures. In order to achieve good conductivity of the mold, a 100 nm thick of Pt film was deposited by RF magnetron sputtering on the mold surface to ensure good conductivity on the mold.

All chemicals were of analytical grade and diluted with ultra-pure water. The etchant-forming solution comprised 0.2 M NaF + 0.4 M $NaClO_3$ + 0.6 M $NaClO_4$ + 0.3 M $NaNO_2$ + 0.1 M NaOH. Using constant current polarization, $I = 5$ mA cm^{-2}. The working temperature was maintained in the range 40–45 °C.

The microstructures of the mold and the etched workpiece were characterized by atomic force microscopy (AFM), (Nanoscope IIIa, Digital Instruments) and scanning electron microscopy (SEM), (QUANTA-200).

3 Results and discussion

3.1 The investigation on the "confining-etching" system

A solution containing NaF, $NaClO_3$ and $NaNO_2$ as precursors to generate electrochemically etchants of HF and HNO_3 in situ was used. The NaOH was used as a scavenger as described above. The electrochemical and chemical reactions during the micromachining process are described as follows:

(1) Generation reactions of etchants (on the surface of the mold)

$$ClO_3^- + H_2O \rightarrow ClO_4^- + 2H^+ + e \quad (1)$$

$$NO_2^- + H_2O \rightarrow NO_3^- + 2H^+ + e \quad (2)$$

$$H^+ + F^- \rightarrow HF \quad (3)$$

$$H^+ + NO_3^- \rightarrow HNO_3 \quad (4)$$

Previously, the mechanism of reaction (1) had been studied extensively [33, 34]. The H^+ generated from reactions (1) and (2) combines with F^- and NO_3^- on the surface of the mold to form etchants HF and HNO_3.

(2) Etching reactions (on the surface of the workpiece)

$$Ti + 6HF \rightarrow H_2[TiF_6] + 2H_2 \quad (5)$$

$$Al + 4HNO_3 \rightarrow Al(NO_3)_3 + NO + 2H_2O \quad (6)$$

$$2V + 6HF \rightarrow 2VF_3 + 3H_2 \quad (7)$$

HNO_3 is a well-known passivator for Ti, especially at high concentrations. It can suppress the corrosion of Ti. However, in a solution of "HNO_3 + NaF", a systematic experiment indicated that this solution still corrodes Ti6Al4V rapidly until the concentration of HNO_3 reaches 1 M.

(3) Destruction reaction of etchant (in solution near the surface of the mold)

$$H^+ + OH^- \rightarrow H_2O \quad (8)$$

NO_2^- can also combine with H^+ since HNO_2 is also a weak acid similar to HF. Therefore it is expected that a competition between NO_2^- and F^- for electrogenerated H^+ may occur. In the solution, the following equilibria exist:

$$HNO_2 \rightleftharpoons H^+ + NO_2^-$$

$$K_{a(HNO_2)} = \frac{[H^+][NO_2^-]}{[HNO_2]} = 5.13 \times 10^{-4}$$

$$HF \rightleftharpoons H^+ + F^- \quad K_{a(HF)} = \frac{[H^+][F^-]}{[HF]} = 6.61 \times 10^{-4}$$

where K_a is the ionization constant of the acid. According to the above equations NO_2^- has even stronger ability to combine with H^+ than F^-. For example, if 1 mol L^{-1} of $[H^+]$ is added to a neutral solution of 1 mol L^{-1} NaF, the F^- will associate with H^+ to form HF, and finally $[HF] \approx 0.99935$ mol L^{-1} while $[H^+] \approx 0.00065$ mol L^{-1}. On the other hand, if 1 mol L^{-1} of $[H^+]$ is added to a neutral solution of 1 mol L^{-1} $NaNO_2$, the NO_2^- will also associate with H^+ to form HNO_2 and finally $[HNO_2] \approx 0.9995$ mol L^{-1} and $[H^+] \approx 0.0005$ mol L^{-1}. Apparently, NO_2^- has a greater tendency to combine with H^+. In addition, if the concentration of the electrogenerated H^+ is sufficiently high, a decomposition reaction, $H^+ + NO_2^- \rightarrow HNO_2 \rightarrow NO\uparrow + NO_2\uparrow + H_2O$, may take place, which will lead to more H^+ being consumed by NO_2^-.

From thermodynamic data it is possible that there exists another etching reaction: $Al + 6HNO_2 \rightarrow Al(NO_2)_3 + 3NO + 3H_2O$.

Figure 1 shows the cyclic voltammetric (CV) curves of a polycrystalline Pt electrode in different electrolytes. Curve 1 corresponds to the electrolyte composed of 0.2 M NaF + 0.2 M $NaClO_3$. The oxidation peak with a current (I_{p1}) of 3.71×10^{-3} A cm^{-2} at the peak potential (φ_{p1}) of 1.53 V was observed. When the potential was higher than 1.56 V, the dissociation reaction of water ($2H_2O - 4e = O_2 + 4H^+$) took place, and oxygen bubbles evolved on the

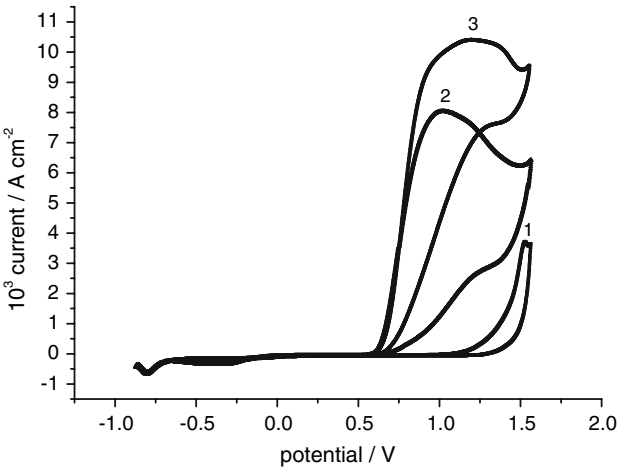

Fig. 1 Cyclic voltammograms of polycrystalline Pt electrode in different electrolytic solution. Scan rate: 10 mV s^{-1}. (1) 0.2 M NaF + 0.2 M $NaClO_3$; (2) 0.2 M NaF + 0.1 M $NaNO_2$; (3) 0.2 M NaF + 0.2 M $NaClO_3$ + 0.1 M $NaNO_2$

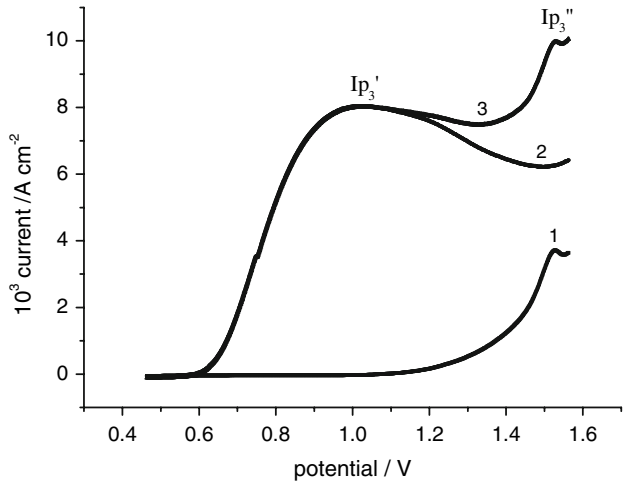

Fig. 2 Cyclic voltammograms of polycrystalline Pt electrode in two electrolytic solution and their sum curve. Scan rate: 10 mV s^{-1}. (1) 0.2M NaF + 0.2M $NaClO_3$; (2) 0.2M NaF + 0.1M $NaNO_2$; (3) The sum of curve (1) and (2)

electrode. In the case of curve 2 in the electrolyte of 0.2 M NaF + 0.1 M $NaNO_2$, an oxidation peak with a current (I_{p2}) of 8.04×10^{-3} A cm^{-2} was observed at the peak potential (φ_{p2}) of 1.00 V. It can be shown that NO_2^- has higher anodic oxidation reaction rate than ClO_3^-. However, in the electrolyte containing two oxidable precursor of 0.2 M NaF + 0.2 M $NaClO_3$ + 0.1 M $NaNO_2$, as shown in curve 3, theoretically it should have two oxidation peaks, but its only oxidation peak φ_{p3} with a current (I_{p3}) of 1.05×10^{-2} A cm^{-2} is at 1.2 V, which is higher than φ_{p2} and less than φ_{p1}. The peak is a very wide one. When the potential moved positively to 1.6 V, oxygen bubbles also began to evolve on the electrode. There was no second peak in curve 3. This is likely due to interaction between ClO_3^- and NO_2^- radicals on the electrode surface during adsorbing and discharging processes, which leads to the oxidation peaks of two precursors shifting and tending to a narrow potential range. A synergistic effect between ClO_3^- and NO_2^- for electrochemical oxidation can be observed from the CV curves. Corresponding to the potential φ_{p3} of curve 3, the current values on the curve 1 and curve 2 are $I_1 = 1.48 \times 10^{-4}$ A cm^{-2} and $I_2 = 7.52 \times 10^{-3}$ A cm^{-2} respectively. Obviously, I_{p3} is much larger than the sum of I_1 and I_2. This may be caused by the catalysis of ClO_3^- to the electrooxidation of NO_2^- on the electrode surface.

To understand the interaction, A algebraic summation of curve 1 and curve 2 of Fig. 1 is calculated and shown in Fig. 2 (here only the positive scanning segments of curve 1 and curve 2 are calculated). Curve 3 of Fig. 2 represents the summation curve of curves 1 and 2. It has two oxidation current peaks, I_{p3}' and I_{p3}'', corresponding to the peak potential values of curve 1 and curve 2 respectively. Curve 3 of Fig. 2 is very different from the curve 3 of Fig. 1 obtained by experiment. It suggests that the effect of combining the precursors of $NaClO_3$ and $NaNO_2$ is not simply through the summation of the effects of each. The interactions between the two precursors of H^+ in the electrode processes made their behavior different from that when they are separated.

During the etching process, some hydrogen evolved on the titanium surface, which may influence the thickness of etchant layer. A small amount of surfactant (hexadecyl trimethyl ammonium chloride, 0.1 g L^{-1}) was added to facilitate hydrogen bubble detachment and evolution.

3.2 Electrochemical micromachining on Ti6Al4V alloy

Figure 3 illustrates a significant improvement in resolution caused by scavenger during the micro hole machining. Figure 3a is an SEM image of a Pt tip used as mold for machining Ti alloy. Its apex-diameter is about 48 μm. Figure 3b is the microstructure machined on the surface of titanium alloy with the above Pt tip as the etchant layer was

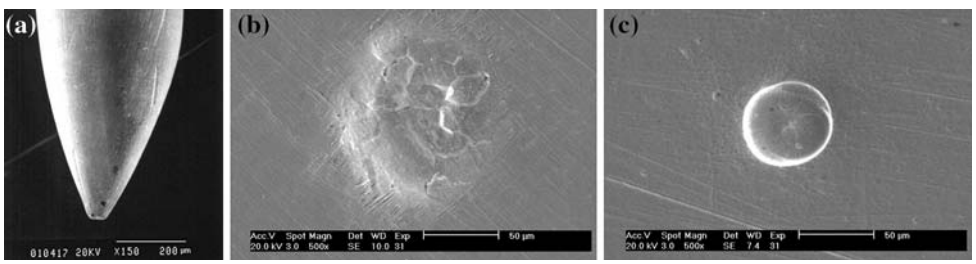

Fig. 3 (**a**) SEM image of a mold for etching titanium alloy—Pt tip. Apex-diameter is about 48 μm, (**b**) SEM image of the microstructure etched on the surface of titanium alloy with above Pt tip as the etchant layer not being confined. The pit-diameter is about 131 μm. The etching solution composed of 0.2 M NaF + 0.4 M $NaClO_3$ + 0.6 M $NaClO_4$ + 0.3 M $NaNO_2$. Machining time $t = 25$ min, (**c**) SEM image of the microstructure etched on the surface of titanium alloy with above Pt tip as the etchant layer being confined by scavenger NaOH. The surface hole-diameter is about 54 μm. The etching solution composed of 0.2 M NaF + 0.4 M $NaClO_3$ + 0.6 M $NaClO_4$ + 0.3 M $NaNO_2$ + 0.1 M NaOH. Machining time $t = 25$ min

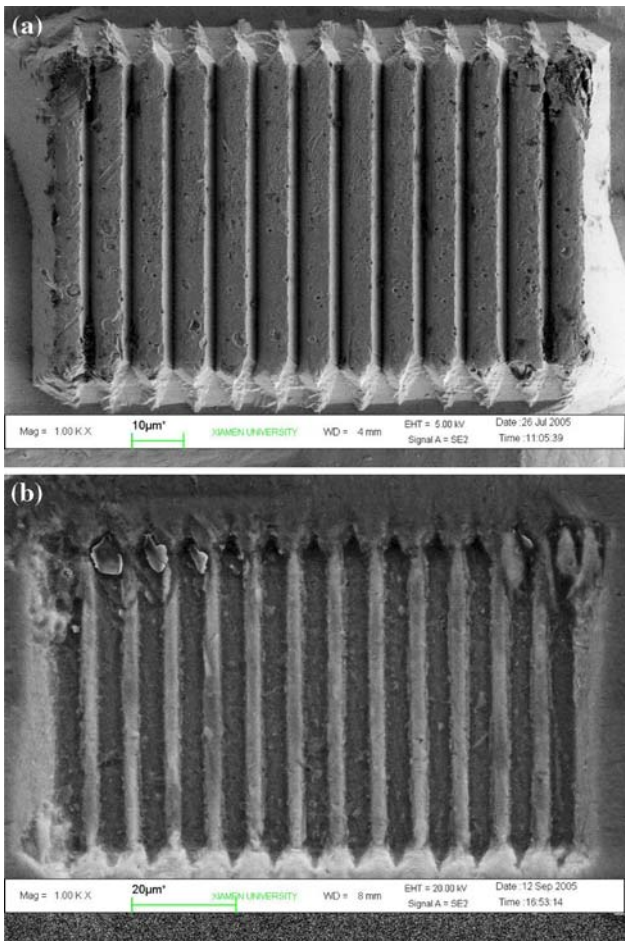

Fig. 4 (**a**) SEM image of the mold with trapezoidal gear-like microstructure, (**b**) Trapezoidal slot microstructure fabricated on Ti alloy surface in the solution composed of 0.2 M NaF + 0.4 M $NaClO_3$ + 0.6 M $NaClO_4$ + 0.3 M $NaNO_2$ + 0.1 M NaOH. Machining time $t = 35$ min

not confined by scavenger. It is merely a pit. The pit-diameter is about 131 μm. Figure 3c shows a micro hole machined on the surface of titanium alloy with the Pt tip The etchant layer was confined by NaOH scavanger. The surface hole-diameter is about 54 μm. Obviously, the resolution is enhanced greatly by the scavenger.

Figure 4a shows the trapezoidal gear-like microstructures on another mold used for micromachining. Figure 4b shows the mirror-image replica microstructures of trapezoidal slots fabricated on Ti6Al4V alloy with the mold. Thirteen slots were fabricated, which is approximately the negative copy of thirteen protruding teeth on the mold surface. In the top left corner of Fig. 4b some reaction product remains in the slots. This should be removed by rinsing the workpiece completely after etching.

Figures 5a, b are the AFM images and their section profiles of the microstructures on the mold and etched on Ti6Al4V, respectively.

Figure 5a shows that the width of the teeth on the mold is 2.45 μm (b_1), while the corresponding feature width etched on titanium is 3.50 μm (b_2). From the difference of the corresponding feature dimensions between the mold and the etched pattern, the resolution of the micromachining can be estimated to be $\Delta b = (b_2 - b_1)/2 = 0.503$ μm.

Finally, to obtain a higher micromachining resolution, it is necessary to adjust the other processing parameters such as the current density, the concentration of ClO_3^- and OH^-. A current density (4–6 mA cm^{-2}) was needed to achieve a good surface roughness after micromachining. Too low current density may lead to non-uniform corrosion on the etched surface, while too high current density causes decreased resolution. Theoretically, an increase in $NaClO_3$ concentration enhances the ClO_3^- conversion rate and generates more H^+, which leads to high etching rate. But the experiments indicate that if the concentration of $NaClO_3$ is too high (>0.6 M in present solution composition), it is difficult to obtain the microstructures. Too high scavenger (NaOH) concentration also did not produce microstructures.

Figure 5b shows that the etched titanium surface is still rough; however, further optimization of the process parameters or appropriate post-treatment steps such as electropolishing [35] will improve the smoothness of the etched surface.

4 Conclusion

The results demonstrate that the confined etchant layer technique (CELT) has potential for machining complex three-dimensional microstructures on Ti alloy (Ti6Al4V). It can be used in a batch process with fewer steps compared to multiple steps in photolithography technique. CELT has low cost as compared with high energy beam machining. Its micromachining resolution depends mainly on the rate of the scavenging reaction. The electrolyte system containing $NaClO_3$, $NaNO_2$ and NaF is suitable for the generation of etchants of HF and HNO_3 in situ. Sub-micrometer resolution can be obtained using NaOH as an effective scavenger. Further experiments to achieve high-aspect-ratio complex three-dimensional microstructures for the Ti alloy will make the fabrication of novel micro devices possible and will extend the functionalities of MEMS. Of course, CELT also has some limits. For example, its machining rate is lower than that of high energy beam machining and EMM. After a certain duration the etching rate becomes slow and it is necessary to lift the mold for some distance and replace it periodically to allow ionic diffusion. In addition, contact between the mold and the workpiece should be avoided during micromachining.

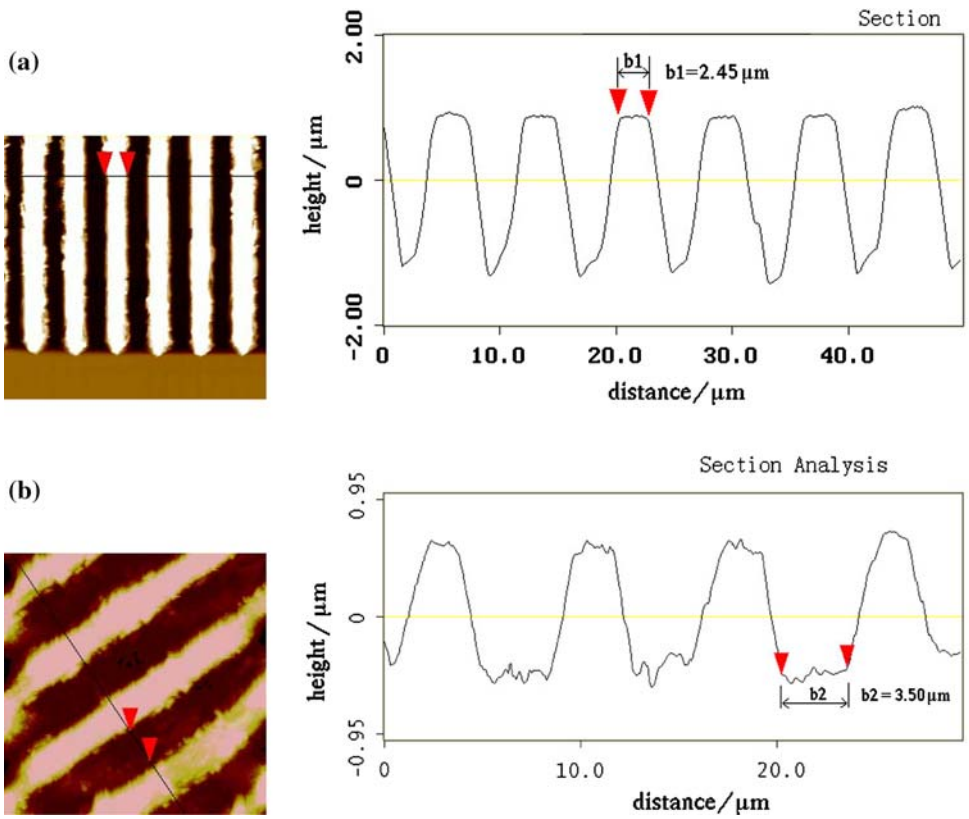

Fig. 5 (**a**) AFM image and section of the microstructure on the mold, (**b**) AFM image and section of the microstructure fabricated on Ti alloy surface. The etching solution composed of 0.2 M NaF + 0.4 M $NaClO_3$ + 0.6 M $NaClO_4$ + 0.3 M $NaNO_2$ + 0.1 M NaOH

Acknowledgements This work was supported by Foundation of 863 Plan of China (2002AA40170), Foundation of the Material Research Center of Jiangxi Province (ZX200301013), Foundation of the Jiangxi Province Department of Education and the Aeronautical Science Foundation. A. Attia would like to thank Xiamen University for financial support.

References

1. Mineta T, Mitsui T, Watanabe Y, Kobayashi S, Haga Y, Esashi M (2001) Sens Actuators A Phys 88:112
2. Arias F, Oliver SRJ, Xu B, Holmlin RE et al (2001) J Microelectromech Syst 10:107
3. Cagatay S, Koc B, Uchino K (2003) IEEE Trans Ultrason Ferroelectr Freq Control 50:782
4. Friend J, Nakamura K, Ueha S (2004) IEEE ASME Trans Mechatron 9:467
5. Serre C, Yaakoubi N, Martínez S et al (2005) Sens Actuators A Phys 123–124:633
6. Lai YJ, Bordatchev EV, Nikumb SK et al (2006) J Intelligent Mater Syst Struc 17:919
7. Becker EW, Ehrfeld W, Hagmann P, Maner A, Münchmeyer D (1986) Microelectron Eng 4:35
8. Romankiw LT (1997) Electrochim Acta 42:2985
9. Leith SD, Schwartz DT (1999) J Microelectromech Syst 8:384
10. Rajan N, Mehregany M, Zorman CA et al (1999) J Microelectromech Syst 8:251
11. Zant PV (2000) Microchip fabrication: a practical guide to semiconductor processing, 4th edn, chapter 13. The McGraw-Hill Companies, Inc
12. Plummer JD, Deal MD, Griffin PB (2000) Silicon VLSI technology: fundamentals, practice and modeling, chapter 2. Pearson Education, Inc
13. Datta M, Romankiw LT (1989) J Electrochem Soc 136:285C
14. Datta M (1998) IBM J Res Develop 42:655
15. Datta M, Landolt D (2000) Electrochim Acta 45:2535
16. Datta M (1995) J Electrochem Soc 142:3801
17. Madore C, Piotrowski O, Landolt D (1999) J Electrochem Soc 146:2526
18. Zinger O, Chauvy P-F, Landolt D (2003) J Electrochem Soc 150: B495
19. Kwak J, Bard AJ (1989) Anal Chem 61:1221
20. Mandler D, Bard AJ (1989) J Electrochem Soc 136:3143
21. Hüsser OE, Craston DH, Bard AJ (1989) J Electrochem Soc 136:3222
22. Mandler D, Bard AJ (1995) J Electrochem Soc 142:L82
23. Schuster R, Kirchner V, Allongue P, Ertl G (2000) Science 289:98
24. Kirchner V, Cagnon L, Schuster R, Ertl G (2001) Appl Phys Lett 79:1721
25. Kock M, Kirchner V, Schuster R (2003) Electrochim Acta 48:3213
26. Trimmer AL, Maurer JJ, Schuster R, Zangari G, Hudson JL (2005) Chem Mater 17:6755
27. Aimi MF, Rao MP, MacDonald NC (2004) Nat Mater 3:103
28. Zu YB, Xie L, Mao BW, Mu JQ, Tian ZW (1998) Electrochim Acta 43:1683
29. Sun JJ, Huang HG, Tian ZQ, Xie L, Luo J, Ye XY, Zhou ZY, Xia SH, Tian ZW (2001) Electrochim Acta 47:95
30. Zhang L, Ma XZ, Zhuang JL et al (2007) Adv Mater 19:3912
31. Jiang LM, Liu ZF, Tang J, Zhang L, Shi K, Tian ZQ, Liu PK, Sun LN, Tian ZW (2005) J Electroanal Chem 581:153

32. Tian ZW, Feng ZD, Tian ZQ, Zhuo XD, Mu JQ, Li CZ, Lin HS, Ren B, Xie ZX, Hu WL (1992) Faraday Discuss 94:37
33. De Nora O, Gallone P, Traini C, Meneghini G (1969) J Electrochem Soc 116:146
34. Osuga T, Fujii S, Sugino K, Sekine T (1969) J Electrochem Soc 116:203
35. Piotrowski O, Madore C, Landolt D (1998) J Electrochem Soc 145:2362